Published in final edited form as:
Crit Care Med. 2013 February ; 41(2): 527–535. doi:10.1097/CCM.0b013e31826ab1f2.

Imaging the Interaction of Atelectasis and Overdistention in Surfactant Depleted Lungs

Maurizio Cereda, MD[1], **Kiarash Emami, PhD**[2], **Yi Xin, MS**[2], **Stephen Kadlecek, PhD**[2], **Nicholas N. Kuzma, PhD**[2], **Puttisarn Mongkolwisetwara, MS**[2], **Harrilla Profka, DVM**[2], **Stephen Pickup, PhD**[2], **Masaru Ishii, MD, PhD**[1,3], **Brian P. Kavanagh, MD, FRCPC**[4], **Clifford S. Deutschman, MD, FCCM**[1], and **Rahim R. Rizi, PhD**[2]

[1]Department of Anesthesiology and Critical Care and Stavropoulos Sepsis Research Program, University of Pennsylvania, Philadelphia, PA, USA

[2]Department of Radiology, University of Pennsylvania, Philadelphia, PA, USA

[3]Johns Hopkins University, Department of Otolaryngology–Head & Neck Surgery, Baltimore, MD, USA

[4]Departments of Critical Care Medicine and Anesthesia, Hospital for Sick Children, University of Toronto, Toronto, ON, Canada

Abstract

Objective—Atelectasis and surfactant depletion may contribute to greater distension – and thereby injury – of aerated lung regions; recruitment of atelectatic lung may protect these regions by attenuating such overdistension. However, the effects of atelectasis (and recruitment) on aerated airspaces remain elusive. We tested the hypothesis that during mechanical ventilation, surfactant depletion increases the dimensions of aerated airspaces and that lung recruitment reverses these changes.

Design—Prospective imaging study in an animal model.

Setting—Research imaging facility

Subjects—27 healthy Sprague Dawley rats

Interventions—Surfactant depletion was obtained by saline lavage in anesthetized, ventilated rats. Alveolar recruitment was accomplished using positive end-expiratory pressure (PEEP) and exogenous surfactant administration.

Measurements and Main Results—Airspace dimensions were estimated by measuring the apparent diffusion coefficient (ADC) of ^{3}He, using diffusion-weighted hyperpolarized gas magnetic resonance imaging (MRI). Atelectasis was demonstrated using computerized tomography (CT) and by measuring oxygenation. Saline lavage increased atelectasis (increase in non-aerated tissue from 1.2 to 13.8% of imaged area, P<0.001), and produced a concomitant increase in mean ADC (~33%, P<0.001) *vs*. baseline; the heterogeneity of the CT signal and the variance of ADC were also increased. Application of PEEP and surfactant reduced the mean ADC

Corresponding Author: Maurizio Cereda, MD, Department of Anesthesiology and Critical Care Perelman School of Medicine at the University of Pennsylvania, Dulles 773, 3400 Spruce Street Philadelphia, PA 19104-4283. Tel: (215) 300-1519, maurizio.cereda@uphs.upenn.edu.

The authors have not disclosed any potential conflicts of interest

COMPETING INTERESTS
Dr. Kiarash Emami is currently affiliated with Polarean, Inc. in Durham, NC.

(~23%, P<0.001), and its variance, in parallel to alveolar recruitment (*i.e.* less CT densities and heterogeneity, increased oxygenation).

Conclusions—Overdistension of aerated lung occurs during atelectasis, is detectable using clinically relevant MRI technology, and could be a key factor in the generation of lung injury during mechanical ventilation. Lung recruitment by higher PEEP and surfactant administration reduces airspace distension.

Keywords

Imaging/MRI; ARDS; Ventilator-Induced Lung Injury; Alveolar Recruitment; Artificial Respiration; Hyperpolarized Gas

INTRODUCTION

Ventilator induced lung injury (VILI) occurs because of excessive tissue distension during mechanical ventilation (1). Surfactant depletion or inactivation increases susceptibility to VILI (2). One consequence of surfactant depletion is atelectasis, which may be a key reason why recruitment and positive end-expiratory pressure (PEEP) attenuate VILI in experimental studies (2–4). One postulated mechanism whereby atelectasis contributes to lung injury is 'atelectrauma', hypothesized to reflect the opening and closing of airways in atelectatic lung during mechanical ventilation (5–7); this repetitive airway strain may initiate local injury that could progress through adjacent tissue (5). Support for this mechanism includes demonstration of small airways injury in isolated lungs that is attenuated in the presence of PEEP (2, 5). According to this construct, recruitment attenuates VILI by stabilizing airspace opening in areas of atelectasis, thus preventing atelectrauma. However, morphometric data have not uniformly demonstrated airway instability (8, 9). A different view, supported by computed tomography (CT) human studies is that atelectasis results in a concentration of the tidal volume (V_T) into a smaller area of aerated (*i.e.* non-atelectatic) lung that becomes over-expanded (10, 11). In this model, the presence of atelectasis contributes to injury by decreasing the size of the 'available' lung and thus injury develops in the aerated regions. Support for this proposal comes from laboratory (12) and clinical (13) data suggesting that the preponderance of alveolar injury occurs in the aerated rather than atelectatic lung regions.

It is likely that both atelectrauma and overdistension contribute to the genesis of VILI. For this reason, it would be valuable to better quantify and understand the relevance of overdistension, since recruitment of atelectatic lung could attenuate VILI by decreasing over-expansion of aerated airspaces. However, some of the therapies that decrease atelectasis (i.e. PEEP) may potentially increase the expansion of aerated airspaces, thus worsening VILI. All approaches to understanding the role of atelectasis and overdistension in lung injury involve serious challenges including model specificity (5), topographic distribution (12), real-time imaging (7), assumptions about cellular metabolism and injury (13), and applicability to humans. Nevertheless, regional airspace sizes can be estimated *in vivo* during mechanical ventilation by measuring the apparent diffusion coefficient (ADC) of helium-3 (^{3}He) using diffusion-weighted hyperpolarized gas magnetic resonance imaging (HPG MRI) (14). ADC provides a non-invasive, clinically applicable estimate of the size of ventilated airspaces on the acinar scale (15), which is not accessible by clinical CT methodologies. This technique can provide measures of the mean "and variance of" ADC values in sampled lung regions as well as illustrative 'maps' of the distribution of ADC.

We hypothesized that atelectasis resulting from surfactant depletion would result in reciprocal airspace volume expansion (expressed as increased mean ADC) in *in vivo* rats ventilated with low PEEP. We further hypothesized that alveolar recruitment would reduce

overdistension by recovering atelectatic lung. We administered surfactant and PEEP to discriminate the responses of ADC to recruitment with and without rising PEEP. In this study we used CT to quantify atelectasis and confirm the occurrence of recruitment in this model.

MATERIALS AND METHODS

Animals

Studies were performed on healthy, male Sprague Dawley rats (n=27, 420±60g), following approval by the local Institutional Animal Care and Use Committee. Animal care and anesthesia was as previously described (16). The experimental design is outlined in Figure 1. Briefly, general anesthesia was induced and maintained with intraperitoneal pentobarbital (40–60 mg/kg), the trachea intubated (14-gauge catheter; BD, Franklin Lakes, NJ), and the glottis sealed (DAP Products Inc., Baltimore, MD) to prevent gas leak (17). Paralysis was obtained with pancuronium bromide (1 mg/kg IV; Abbot Labs, North Chicago, IL) after connection to the mechanical ventilator. Airway pressure was recorded using a fiber-optic sensor (Samba Sensors AB, Sweden), and heart rate and peripheral oxygen saturation (SpO_2) levels monitored (Nonin Medical, Inc. Plymouth, MN). Body temperature was maintained at 37 °C by warm air-flow and after the final set of observations the animals were removed from the scanner and euthanized by lethal pentobarbital injection.

Experimental Outline

Three series of experiments were performed (Figure 1). To measure the effects of surfactant depletion on ADC, 10 animals (Series 1) underwent HPG MRI at PEEP 0 cmH_2O before and after saline lavage. In five of these rats, images were obtained three times after lavage to verify repeatability of the ADC measurement. Peak inspiratory pressure (PIP) was measured immediately prior to each ADC acquisition and used for dynamic compliance [$Cdyn = V_T/(PIP - PEEP)$] measurements.

10 rats (Series 2) received saline lavage with identical procedure as Series 1 animals and were used to study the effects of recruitment by PEEP and exogenous surfactant on ADC. Animals were imaged with and without PEEP at baseline, following saline lavage, and after intratracheal instillation of surfactant (Figure 1). Seven additional animals (Series 3) were used to verify atelectasis and document the effects of PEEP and surfactant on alveolar recruitment. This was measured from lung CT densities and SpO_2. Animals underwent a similar protocol as in Series 2 (Figure 1), except that CT images “instead of ADC” were acquired at each time point.

Surfactant Depletion

After baseline imaging, saline lavage was performed in all rats as previously described (12). Animals were briefly disconnected from the ventilator and lavaged with 30 mL/kg of warmed (37 °C) saline, instilled using a syringe attached to the endotracheal tube. The saline was then gently retrieved by slowly suctioning through the same syringe, the total amount recovered was recorded and was lower than two ml in all animals. The lavage procedure was performed three times, at 5-minute intervals, followed by a 20 minutes period of stabilization at PEEP 4 cmH_2O and with FIO_2 of 1.0, following which the animal was returned to the scanner (same position as before) and images were obtained.

Exogenous Surfactant

In Series 2 and 3 animals, a single intratracheal dose (50 mg/kg) of Bovine Lipid Extract Surfactant (BLES Biochemicals Inc. London, ON, Canada) was injected slowly while

maintaining the animal 45 degrees head-up, followed by reconnection to the ventilator. Imaging was repeated following stabilization for 20 minutes.

Mechanical Ventilation

All rats were ventilated with an MRI-compatible, custom-built small animal ventilator capable of delivering volumes with an accuracy of ± 100μl (16). Animals were placed supine in the CT or MRI scanner and ventilated (V_T 10 mL/kg, respiratory rate 60 per minute, inspiratory time 30%, PEEP 0 cmH_2O, and FiO_2 0.21). Except for PEEP and FiO_2 when specified, all ventilator settings were left unchanged throughout the course of the experiment. A recruitment maneuver (serial increases of PEEP in increments of 3 cmH_2O, each for 30 sec., up to 15 cmH_2O) was performed prior to each series of image acquisitions to standardize lung recruitment and volume history. Except for ADC acquisitions, FiO_2 of 1.0 was delivered to maintain adequate arterial oxygenation during and after saline lavage, until the end of the experiments.

In Series 1, PEEP of zero only was applied during measurements. In Series 2 and 3, ADC and CT images were obtained at all levels of applied PEEP (0–15 cmH_2O, Series 2; 0–12 cmH_2O Series 3; 0–9 cmH_2O after surfactant). In control conditions, only PEEP levels of 0 and 9 cmH_2O were applied, in order to verify the effect of lung inflation on ADC. Each level of PEEP was applied for 3 minutes prior to CT or ADC imaging. Higher levels of PEEP were poorly tolerated by healthy rats or after surfactant administration (pilot data, not shown) and were therefore avoided.

HPG MRI Protocol

HPG MRI was performed using a diffusion-weighted gradient echo pulse sequence. End-inspiratory images were obtained following ventilation with a mixture of hyperpolarized ^3He and O_2. At 30 breaths before each image acquisition, the inspired gas was switched to a mixture of $^4He:O_2$ (4:1) in order to standardize the alveolar gas composition and eliminate the dependence of ADC on residual gas volume (18). The source gas was then switched to HP $^3He:O_2$ (4:1) for five breaths prior to ADC imaging, which was performed during a 5-second inspiratory pause and after a 1-sec delay time to allow uniform inspired gas distribution. Imaging was performed with a 50-cm bore 4.7-T MRI scanner (Varian Inc., Palo Alto, CA) equipped with 12-cm 25 G/cm gradients and a quadrature 8-leg birdcage RF coil with internal diameter of 7 cm (Stark Contrast, Erlangen, Germany) tuned to the ^3He resonance frequency of 152.95 MHz. ^3He gas was hyperpolarized to approximately 30% over 14 hours using a commercial prototype (IGI.9600. He, GE Healthcare, Durham, NC) (19). Rats were placed supine in the coil inside the MRI scanner. In all animals, ADC imaging was performed on axial or coronal slices using an interleaved diffusion-weighted gradient echo imaging pulse sequence with Cartesian centric *k*-space sampling using the following parameters: planar resolution =0.94×0.94 mm^2, field of view (FOV) =6×6 cm^2, flip angle α =2–3°, repetition time (TR) =4.5 mSec, and echo time (TE) =3.3 mSec (14, 16). In Series 1, the 20-mm axial slice was positioned right underneath the heart in order minimize the cardiac motion artifacts and maximize the lung parenchyma included in the imaged slab. In Series 2, imaging was performed on two 10-mm coronal slices, one anterior and one posterior. A single-breath high-resolution coronal ^3He spin density (ventilation) image was also acquired in this subset of animals before and after saline lavage at a planar resolution of 0.47×0.47 mm^2 (all imaging parameters similar to ADC protocol except for α =5°, TR =3.2 mSec and TE =1.6 mSec). Each set of ADC acquisitions comprised eight diffusion-weighted images corresponding to different diffusion gradient factors (*b*-values) ranging between 0 and 6 cm^2/s (with b =0 repeated as the first and last image) (20). Diffusion weighting was performed along the left-right direction of the rat body, using

diffusion time Δ =1 mSec and gradient duration δ =200 μSec all with a fixed ramp time of τ =180 μSec.

CT Protocol

High-resolution, end-inspiratory CT scans were acquired using a micro-CT scanner (ImTek MicroCAT II; Knoxville, TN) with FOV =5.27×5.27 cm^2 and an isotropic resolution of 103×103×103 μm^3. To avoid blurring due to respiratory motion, only one view per breath was acquired during each 500 mSec ventilator-gated breath-hold. Image reconstruction was performed. For qualitative comparison with ADC maps, anterior and posterior coronal slices were thus reconstructed with a proprietary program supplied by the scanner manufacturer (MicroCAT: Image Reconstruction, Visualization, and Analysis; Knoxville, TN).

Data Analysis

All analysis was performed using MATLAB (Mathworks, Natick, MA) codes developed in the authors' laboratory. ADC was analyzed on a pixel-by-pixel basis at a planar resolution of approximately 0.94×0.94 mm^2. The acquired signal was bias-corrected for the background noise (21). The signal-to-noise (SNR) threshold was iteratively varied between 5 and 20 for each image and the highest threshold value was selected such that the entire lung parenchyma was retained after masking the low SNR pixels. Time evolution of signal intensity of valid pixels was then fit to a standard equation to yield maps of regional ADC values (16). Mean, standard deviation (STD), skewness, and kurtosis were calculated for each imaged slice.

Quantitative analysis of CT densities was performed using established methods. Briefly, alveolar recruitment was quantified from shifts of tissue between compartments with predefined density ranges (11, 22, 22). Two-dimensional regions of interest were identified on images by manually contouring around the profile of both lungs excluding the heart and the major vessels. For each region of interest, frequency histograms of Hounsfield Units (HU) values were extracted, mean and STD were obtained. Such distributions were partitioned among compartments of different aeration: [a] non-aerated (−100 to +100 HU); [b] poorly aerated (−500 to −101 HU); [c] normally aerated (−900 to −501 HU); and, [d] hyperinflated (−1000 to −901 HU). Each compartment was measured as the percentage of the total slice area occupied. Alveolar recruitment was assessed from increases in the normally aerated compartment and decreases in the non-aerated one.

For statistical analysis, group mean and standard deviation values of all the computed quantities were calculated. Relative changes of measured quantities were compared using a repeated measurements analysis of variance followed by *post hoc* comparisons between conditions, using paired *t*-test and the Bonferroni correction for multiple comparisons when appropriate. Statistical significance was set at $P < 0.01$.

RESULTS

Series 1 — Effect of Surfactant Depletion on ADC

The baseline values of PIP and ADC, and the standard deviation of ADC (Table 1) were comparable to previously published values in healthy rats of similar weight and comparable ventilator settings (16). Figure 2 shows the ^{3}He density (Figure 2-A) and ADC (Figure 2-B) maps of the mid-axial slices of two representative rat lungs. The frequency distribution histograms (Figure 2-C) confirm that before surfactant depletion the distribution of ^{3}He ADC was unimodal and skewed towards smaller values, reflecting a preponderance of patent smaller airspaces.

Surfactant depletion resulted in an increased PIP, decreased dynamic compliance (Cdyn), and higher mean ADC (by over 30%, P<0.001), compared with pre-lavage values (Table 1). ^{3}He density maps (Figure 2-A) show an overall lower signal, indicating reduced airspace aeration. The heterogeneity of ADC signal, indicative of non-uniform airspace distension, was increased after surfactant depletion (Figure 2-B); this is reflected also in the larger standard deviation (P<0.002) and smaller kurtosis (P<0.001) of the ADC frequency distributions (Table 1; Figure 2-C). The skewness of ADC frequency distributions was decreased post-lavage (P<0.001, Table 1) consistent with an increased contribution of larger *vs.* smaller airspaces to the overall ADC distribution. The intra-subject variation of ADC measurements following saline lavage was less than 6% (Table S1).

Series 2 — Effects of PEEP and Exogenous Surfactant on ADC

Following surfactant depletion the overall ADC values, as well as the heterogeneity of the regional ADC distribution, were increased (Figure 3). ADC values obtained from the posterior and anterior coronal slices followed similar trends with minimal quantitative variations among slices and were therefore combined and expressed as a single mean (± SD) for each study condition (Figure 4). The mean ADC increased by 32.6% after lavage (Figure 4, P<0.0001); the magnitude of this effect was slightly greater in the posterior *vs.* anterior slices (P<0.01, Figure S1). The regional gas content and aeration defects (*i.e.* airspaces not reached by the tracer gas) were visualized by high resolution ^{3}He density maps (Figure 3-A). Following surfactant depletion, aeration defects were more prominent, particularly in the posterior slice.

Before surfactant depletion, application of PEEP (9 cmH_2O) increased the mean ADC values (Figure 4). After lavage, PEEP (in the absence of surfactant) decreased the overall ADC (Figure 4) and, at PEEP levels up to 15 cm H_2O, converted the ADC distribution to a more homogenous pattern (Figure 3-B). Aeration defects in ^{3}He density scans were also decreased at high PEEP (Figure 3-A). At zero PEEP, administration of surfactant had minimal effect on overall ADC (Figures 3-B, 4), although it was slightly reduced (approximately 6%, P<0.001) in the posterior slices (Figure S1). Combining surfactant with PEEP decreased mean ADC by 22.7% (P<0.01) and resulted in a greater (approx. 11%, P<0.01) decrease in ADC *vs.* PEEP (9 cmH_2O) alone (Figure 4). In the context of both PEEP and surfactant, mean ADC values were comparable to healthy conditions (Figure 4); at mid-range levels of PEEP (*i.e.* 9 cmH_2O), the ADC dispersion was normalized (Figure S2) and the ADC maps were almost identical to baseline (Figure 3-B). In contrast to the slightly predominant posterior (dorsal) region impact of surfactant depletion (saline lavage) and replacement on ADC, the effects of PEEP were similar in anterior *vs.* posterior slices (Figure S1). Aeration defects were virtually eliminated by the combination of PEEP 9 cmH_2O and surfactant, reflecting the successful recruitment of atelectatic areas (Figure 3-A). Dynamic representation of ^{3}He density maps (see animations in the Supplemental Digital Content) obtained in one animal by stepwise increases in PEEP (3 cmH_2O increments) confirmed heterogeneous lung aeration after surfactant depletion (*vs.* baseline), and progressively disappearing aeration defects after administration of surfactant.

Series 3 — Alveolar Recruitment

Saline lavage caused a significant increase in tissue density on CT scans (Figure 5), which was related to an increase in poorly aerated and non-aerated lung tissue at the expense of the normally aerated compartment (Figure 6). PEEP induced significant alveolar recruitment, suggested by lower densities (Figure 5) and quantified by increased aeration distributed over all lung regions (Figure 6). CT imaging indicated that the rank order for effectiveness in recruitment was: Surfactant plus PEEP > PEEP > Surfactant (Figure 6). As observed with estimation of ADC, the effects of lavage, PEEP, and surfactant on CT density was

qualitatively comparable among slices but areas of non-aerated tissue were more pronounced in the posterior slices (Figure S3). PEEP induced regional overdistension (apparent in CT imaging) only in the pre-lavage (normal) lungs, and not in any of the post-lavage conditions. PEEP and surfactant decreased dispersion (STD) of CT densities (Figure S2).

Before surfactant depletion, increasing PEEP was not associated with changes in SpO_2 (Figure 7). Surfactant depletion resulted in a high level of PEEP (15 cmH_2O) needed in order to achieve a SpO_2 of 95%. In contrast, the SpO_2 response to PEEP following administration of surfactant was a sharp increase in SpO_2 up to 95% which was achieved at PEEP 9 cmH_2O. The airway pressure-time profiles (Figure S4) show upward convexity after surfactant depletion. This convexity, which typically indicates the presence of recruitable lung (23), was attenuated at lower PEEP after surfactant replacement as compared to PEEP alone, which also suggests the facilitating effect of surfactant on recruitment.

DISCUSSION

The results of this study support our hypothesis that with volume-controlled ventilation, surfactant depletion leads to elevated ADC values in aerated regions of the lung. This finding is consistent with two lung unit populations in the setting of atelectasis: atelectatic units and reciprocally volume-expanded airspaces. The overdistension occurred despite moderate V_T, was not identified by CT, and was most prominent at zero PEEP in the dorsal lung regions. PEEP did not increase overdistension; in contrast, recruitment by PEEP and/or exogenous surfactant reduced overdistension.

Interpretation of ADC Measurement

Respiratory gas diffusion maps provide regional information pulmonary airspace dimensions. The current methodology excluded proximal conductive airways from analysis and thus ^3He ADC values primarily reflect small (aerated) airspaces within the acinus (24), where diffusion is the main determinant of gas transport (25). In fact, ADC correlates well with small airway dimensions and alveolar surface density (14, 26). The response of ADC to PEEP at baseline (before lavage) suggests that it is sensitive to changes in airway pressure; this is consistent with the increases in ADC in the current experiments being due to enlarged acinar airspaces. While reproducibility of ADC has been documented in other settings (18, 27, 28), the repeat acquisitions (Table S1) in the current study provide the first confirmation of repeatability in a small animal model of surfactant depletion, thus supporting the reproducibility of our measurements in this model.

A potential limitation of the diffusion-weighted MRI technique is insufficient discrimination between compartments of the acinus, *e.g.* the alveoli *vs.* the alveolar ducts (29). In the presence of atelectasis, initial opening may be dominated by expansion of alveolar ducts (30). However, in the current study, surfactant depletion is associated with CT confirmation of definite regional atelectasis (with minimal contained air), suggesting little likelihood co-localization of atelectasis and air-filled ducts. In addition, with inflation and increasing airway pressure, the ducts may become smaller as alveoli expand (30), suggesting that here, the contribution of duct air filling would be progressively less important. Because alveolar ducts have a less significant role in diffusion than alveoli (31), it is unlikely that duct physiology (or filling) dominates over alveolar distension. More sophisticated diffusion models (32, 33) may help in the future to better define the anatomical correlations of our findings by differentiating between the contribution of alveoli *vs.* the alveolar ducts.

Another potential limitation of ADC is that its interpretation can be problematic when alveolar recruitment is achieved by rising PEEP. Here, further expansion of the previously

aerated airspaces could theoretically be masked by reopening of previously collapsed, smaller airspaces. However, the ADC value within each voxel is a volume-weighted average and is thus more sensitive to the presence of enlarged *vs.* smaller airways (34), thereby mitigating any tendency for ADC to underestimate airspace expansion through elevation of airway pressure (e.g. raising PEEP).

The current results suggest that ADC may provide a valuable tool, complementary to CT, enabling the study of atelectasis on aerated airspaces. In fact, widespread elevated ADC was observed after lavage (Figures 2, 3), while post-lavage CT showed diffusely reduced aeration and no hyperinflation, in the same experimental conditions as in Series 2 (Figures 5, 6). This is likely because CT provides density-weighted measurements of lung tissue/aeration and, as such it may underestimate over-expanded airspaces that abut (or are the result of) atelectatic alveoli.

Saline Lavage Promotes Airspace Expansion

Increases in mean ADC values at end-inspiration after saline lavage can be explained by atelectasis. Development of atelectasis was confirmed by the non-persistent hyperdensities on CT imaging (Figures 5, 6), as well as the recoverable aeration defects in the ^{3}He density maps (Figure 3-A), which have been histologically associated with atelectasis in ventilated mice (35). Animal studies (36) have confirmed that atelectasis is a key characteristic in the saline lavage model; and, although pulmonary edema coexists with atelectasis, the amount of unrecovered saline in our study (<2 mL) was comparable to that observed in a similar model where atelectasis was confirmed by tissue stereology (12). The use of FiO_2 of 1.0 after saline lavage is likely to have further promoted atelectasis (37) although the confounding effectof this factor is likely to be small.

There are important differences between this and previous studies. Previously utilized imaging techniques, such as CT, do not readily permit regional assessment of airspace distention. While other studies showing airspace overexpansion in this model employed a higher V_T (10), we used a moderate V_T. The current findings of increased ADC after saline lavage also document inspiratory overdistension at low PEEP in the context of surfactant depletion. Finally, our results suggest that overdistension was not confined to anterior lung regions and occurred *within* areas of the lungs that appeared to be atelectatic by CT, a finding that was not previously reported.

The topography may be instructive. The post-lavage increase in ADC was larger in the posterior slices (Figure S1), where atelectasis was also prominent (Figure S3). Such co-existence of overdistended lung within areas of atelectasis can be explained by traction from collapsed alveoli (38, 39); such alveolar interdependence may reciprocally expand ventilated airspaces and cause gas redistribution. In fact, morphometric data suggest airspace expansion in close proximity to atelectatic alveoli (7, 30). Comparisons between ADC and CT data are limited by the fact that these imaging techniques were employed (of necessity) in separate groups of animals. However, the ACD data are highly reproducible (Table S1) and the inter-subject variability (ADC and CT data) is small (Figures 4, 6).

Alveolar Recruitment Decreases Airspace Expansion

Surfactant administration and PEEP after saline lavage decreased mean ADC values (Figure 4) and caused the near disappearance of aeration defects on ^{3}He spin density maps (Figure 3-A), especially in the setting of PEEP with surfactant. Furthermore, PEEP and surfactant resulted in almost total recovery (towards baseline) of the ADC standard deviation (Figure S2), reflecting alveolar recruitment; this was corroborated by CT images (Series 3; Figures 5, 6), increased oxygenation (Figure 7), and inspiratory pressure-time profiles (Figure S4).

The decreasing size of aerated airspaces in association with recruitment may reflect resolution of the original overdistension mechanisms. Alveolar recruitment involves an increase in the amount of aerated parenchyma, causing redistribution of inspired gas to a larger pool of ventilated airspaces (40), which should individually be less expanded at end-inspiration. According to this hypothesis, a decrease in airspace dilatation after recruitment can be expected when PEEP remains constant, such as after surfactant instillation or following a recruitment maneuver (16); here, a decrease in the face of rising PEEP may appear paradoxical. However, the latter finding may be explained by release of airspace dilatation that was initially caused by alveolar interdependence (30). Previous *ex vivo* morphometric studies suggested this phenomenon during lung inflation (30, 41, 42), although other investigators have not reported the same findings (43). In our previous study in healthy rats (16), we observed a reduction in mean ADC when PEEP was applied, following the development of atelectasis due to prolonged ventilation at zero PEEP. Following a recruitment maneuver, subsequent application of PEEP caused ADC to increase, which was also observed in the baseline health lungs of the current study. Therefore we infer that a decreasing ADC associated with PEEP characterizes the response of the lungs to alveolar recruitment, while an increasing ADC reflects the physiological inflation of recruited lungs.

The combined effect of PEEP and surfactant on ADC and alveolar recruitment demonstrated a ‘PEEP sparing’ effect of surfactant, a finding consistent with previous studies (44). This effect was particularly evident in the response of arterial saturation after saline lavage, which showed that a normal SpO_2 could be reached at lower PEEP after surfactant (Figure 7).

Limitations and Biological Implications

The current work has important limitations. It does not provide evidence of VILI in areas of high ADC and does not address the presence or possible role of atelectrauma. Indeed, our goal was to identify acute changes in ventilated airspaces in a model that is highly responsive to recruitment attempts and before the onset of VILI. However, surfactant depletion does not reflect the entire spectrum of the pathogenesis of acute lung injury and our results should not be generalized until further experimentation is performed in animal models with prominent inflammation and alveolar consolidation. In addition, the responses of ADC to lavage and recruitment may be affected by the duration of ventilation. In fact, our findings were unlike the observations by Tsuchida *et al.* (12), showing prominently ventral overdistension, a difference that may reflect different V_T (25 vs. 10 ml/kg), the presence of established injury, or study duration. The choice of a small vs. large animal model could have affected the antero-posterior distribution of CT densities. However, the distribution of atelectasis in rats is similar to larger animals (12).

Within experimental confines, the current study provides *in vivo* radiological evidence of airspace expansion in a surfactant-depleted model, extending our work in healthy ventilated rats (16). While lung overdistension “as well as the presence of atelectasis” increases the risk of VILI (1), the current data suggest that atelectasis could contribute to VILI by reciprocal increases in airspace size, a suggestion supported by recent morphometric (12) and clinical data (13); this hypothesis contrasts with previous reports suggesting that atelectasis resulted in injury in the airways in the atelectatic regions (45,46).

The detection of overdistension by ADC “and not by CT” suggests that this phenomenon may be more frequent and more relevant than previously estimated. The response of ADC to recruitment also suggests that attenuation of overdistension may be an important contributor to the beneficial effects of PEEP in surfactant depletion. Our findings of decreased ADC during PEEP suggest that airspaces dilatation is attenuated, rather than worsened, by PEEP

in the presence of marked atelectasis. Such a response might occur in patients with highly recruitable lungs (47), but would not be detectable using conventional clinical techniques.

Supplementary Material

Refer to Web version on PubMed Central for supplementary material.

Acknowledgments

The authors would like to acknowledge BLES Biochemicals Inc. (London, ON, Canada) for donating the surfactant and the Small Animal Imaging Facility at the Department of Radiology, University of Pennsylvania, for its support.

This work was supported by NIH grants R01-HL064741 and R01-HL077241.

References

1. Dreyfuss D, Soler P, Basset G, et al. High inflation pressure pulmonary edema. respective effects of high airway pressure, high tidal volume, and positive end-expiratory pressure. Am Rev Respir Dis. 1988; 137:1159–1164. [PubMed: 3057957]
2. Muscedere JG, Mullen JB, Gan K, et al. Tidal ventilation at low airway pressures can augment lung injury. Am J Respir Crit Care Med. 1994; 149:1327–1334. [PubMed: 8173774]
3. Webb HH, Tierney DF. Experimental pulmonary edema due to intermittent positive pressure ventilation with high inflation pressures. protection by positive end-expiratory pressure. Am Rev Respir Dis. 1974; 110:556–565. [PubMed: 4611290]
4. Steinberg JM, Schiller HJ, Halter JM, et al. Alveolar instability causes early ventilator-induced lung injury independent of neutrophils. Am J Respir Crit Care Med. 2004; 169:57–63. [PubMed: 14695106]
5. Tremblay L, Valenza F, Ribeiro SP, et al. Injurious ventilatory strategies increase cytokines and c-fos m-RNA expression in an isolated rat lung model. J Clin Invest. 1997; 99:944–952. [PubMed: 9062352]
6. Baumgardner JE, Markstaller K, Pfeiffer B, et al. Effects of respiratory rate, plateau pressure, and positive end-expiratory pressure on PaO2 oscillations after saline lavage. Am J Respir Crit Care Med. 2002; 166:1556–1562. [PubMed: 12406831]
7. Halter JM, Steinberg JM, Schiller HJ, et al. Positive end-expiratory pressure after a recruitment maneuver prevents both alveolar collapse and recruitment/derecruitment. Am J Respir Crit Care Med. 2003; 167:1620–1626. [PubMed: 12615628]
8. Mertens M, Tabuchi A, Meissner S, et al. Alveolar dynamics in acute lung injury: Heterogeneous distension rather than cyclic opening and collapse. Crit Care Med. 2009; 37:2604–2611. [PubMed: 19623041]
9. Carney DE, Bredenberg CE, Schiller HJ, et al. The mechanism of lung volume change during mechanical ventilation. Am J Respir Crit Care Med. 1999; 160:1697–1702.
10. Gattinoni L, Pesenti A. The concept of “baby lung”. Intensive Care Med. 2005; 31:776–784. [PubMed: 15812622]
11. Gattinoni L, Pesenti A, Avalli L, et al. Pressure-volume curve of total respiratory system in acute respiratory failure. computed tomographic scan study. Am Rev Respir Dis. 1987; 136:730–736. [PubMed: 3307572]
12. Tsuchida S, Engelberts D, Peltekova V, et al. Atelectasis causes alveolar injury in nonatelectatic lung regions. Am J Respir Crit Care Med. 2006; 174:279–289. [PubMed: 16675780]
13. Bellani G, Guerra L, Musch G, et al. Lung regional metabolic activity and gas volume changes induced by tidal ventilation in patients with acute lung injury. Am J Respir Crit Care Med. 2011; 183:1193–1199. [PubMed: 21257791]
14. Ishii M, Emami K, Xin Y, et al. Regional functional-structure relationships in lungs of an elastase murine model of emphysema. J Appl Physiol. 2011
15. Fain SB, Korosec FR, Holmes JH, et al. Functional lung imaging using hyperpolarized gas MRI. J Magn Reson Imaging. 2007; 25:910–923. [PubMed: 17410561]

16. Cereda M, Emami K, Kadlecek S, et al. Quantitative imaging of alveolar recruitment with hyperpolarized gas MRI during mechanical ventilation. J Appl Physiol. 2011; 110:499–511. [PubMed: 21127207]
17. Spector ZZ, Emami K, Fischer MC, et al. A small animal model of regional alveolar ventilation using HP 3He MRI1. Acad Radiol. 2004; 11:1171–1179. [PubMed: 15530811]
18. Carrero-Gonzalez L, Kaulisch T, Ruiz-Cabello J, et al. Apparent diffusion coefficient of hyperpolarized (3) he with minimal influence of the residual gas in small animals. NMR Biomed. 2012
19. Walker TG, Happer W. Spin-exchange optical pumping of noble-gas nuclei. Rev Mod Phys. 1997; 69:629–642.
20. Osmanagic E, Sukstanskii AL, Quirk JD, et al. Quantitative assessment of lung microstructure in healthy mice using an MR-based 3He lung morphometry technique. J Appl Physiol. 2010; 109:1592–1599. [PubMed: 20798272]
21. Henkelman RM. Measurement of signal intensities in the presence of noise in MR images. Med Phys. 1985; 12:232–233. [PubMed: 4000083]
22. Vieira SR, Puybasset L, Richecoeur J, et al. A lung computed tomographic assessment of positive end-expiratory pressure-induced lung overdistension. Am J Respir Crit Care Med. 1998; 158:1571–1577. [PubMed: 9817710]
23. Ranieri VM, Zhang H, Mascia L, et al. Pressure-time curve predicts minimally injurious ventilatory strategy in an isolated rat lung model. Anesthesiology. 2000; 93:1320–1328. [PubMed: 11046222]
24. Sukstanskii AL, Yablonskiy DA. In vivo lung morphometry with hyperpolarized 3He diffusion MRI: Theoretical background. J Magn Reson. 2008; 190:200–210. [PubMed: 18037313]
25. Weibel ER, Sapoval B, Filoche M. Design of peripheral airways for efficient gas exchange. Respir Physiol Neurobiol. 2005; 148:3–21. [PubMed: 15921964]
26. Tanoli TS, Woods JC, Conradi MS, et al. In vivo lung morphometry with hyperpolarized 3He diffusion MRI in canines with induced emphysema: Disease progression and comparison with computed tomography. J Appl Physiol. 2007; 102:477–484. [PubMed: 16873601]
27. Mathew L, Evans A, Ouriadov A, et al. Hyperpolarized 3He magnetic resonance imaging of chronic obstructive pulmonary disease: Reproducibility at 3. 0 tesla. Acad Radiol. 2008; 15:1298–1311. [PubMed: 18790402]
28. Emami K, Chia E, Kadlecek S, et al. Regional correlation of emphysematous changes in lung function and structure - A comparison between pulmonary function testing and hyperpolarized MRI metrics. J Appl Physiol. 2010
29. Yablonskiy DA, Sukstanskii AL, Leawoods JC, et al. Quantitative in vivo assessment of lung microstructure at the alveolar level with hyperpolarized 3He diffusion MRI. Proc Natl Acad Sci U S A. 2002; 99:3111–3116. [PubMed: 11867733]
30. Bachofen H, Gehr P, Weibel ER. Alterations of mechanical properties and morphology in excised rabbit lungs rinsed with a detergent. J Appl Physiol. 1979; 47:1002–1010. [PubMed: 511700]
31. Mercer RR, Crapo JD. Three-dimensional reconstruction of the rat acinus. J Appl Physiol. 1987; 63:785–794. [PubMed: 3654440]
32. Yablonskiy DA, Sukstanskii AL, Woods JC, et al. Quantification of lung microstructure with hyperpolarized 3He diffusion MRI. J Appl Physiol. 2009; 107:1258–1265. [PubMed: 19661452]
33. Quirk JD, Lutey BA, Gierada DS, et al. In vivo detection of acinar microstructural changes in early emphysema with (3)he lung morphometry. Radiology. 2011; 260:866–874. [PubMed: 21734160]
34. Jacob RE, Minard KR, Laicher G, et al. 3D 3He diffusion MRI as a local in vivo morphometric tool to evaluate emphysematous rat lungs. J Appl Physiol. 2008; 105:1291–1300. [PubMed: 18719237]
35. Thomas AC, Nouls JC, Driehuys B, et al. Ventilation defects observed with hyperpolarized 3He magnetic resonance imaging in a mouse model of acute lung injury. Am J Respir Cell Mol Biol. 2011; 44:648–654. [PubMed: 20595465]
36. Lachmann B, Robertson B, Vogel J. In vivo lung lavage as an experimental model of the respiratory distress syndrome. Acta Anaesthesiol Scand. 1980; 24:231–236. [PubMed: 7445941]

37. Duggan M, McNamara PJ, Engelberts D, et al. Oxygen attenuates atelectasis-induced injury in the in vivo rat lung. Anesthesiology. 2005; 103:522–531. [PubMed: 16129977]
38. Prange HD. Laplace's law and the alveolus: A misconception of anatomy and a misapplication of physics. Adv Physiol Educ. 2003; 27:34–40. [PubMed: 12594072]
39. Mead J, Takishima T, Leith D. Stress distribution in lungs: A model of pulmonary elasticity. J Appl Physiol. 1970; 28:596–608. [PubMed: 5442255]
40. Hickling KG. The pressure-volume curve is greatly modified by recruitment. A mathematical model of ARDS lungs. Am J Respir Crit Care Med. 1998; 158:194–202. [PubMed: 9655729]
41. Lum H, Huang I, Mitzner W. Morphological evidence for alveolar recruitment during inflation at high transpulmonary pressure. J Appl Physiol. 1990; 68:2280–2286. [PubMed: 2384408]
42. Namati E, Thiesse J, de Ryk J, et al. Alveolar dynamics during respiration: Are the pores of kohn a pathway to recruitment? Am J Respir Cell Mol Biol. 2008; 38:572–578. [PubMed: 18096874]
43. Escolar JD, Escolar MA, Guzman J, et al. Pressure volume curve and alveolar recruitment/de-recruitment. A morphometric model of the respiratory cycle. Histol Histopathol. 2002; 17:383–392. [PubMed: 11962742]
44. Krause M, Olsson T, Law AB, et al. Effect of volume recruitment on response to surfactant treatment in rabbits with lung injury. Am J Respir Crit Care Med. 1997; 156:862–866. [PubMed: 9310005]
45. de Prost N, Costa EL, Wellman T, et al. Effects of surfactant depletion on regional pulmonary metabolic activity during mechanical ventilation. J Appl Physiol. 2011; 111:1249–1258. [PubMed: 21799132]
46. Otto CM, Markstaller K, Kajikawa O, et al. Spatial and temporal heterogeneity of ventilator-associated lung injury after surfactant depletion. J Appl Physiol. 2008; 104:1485–1494. [PubMed: 18323462]
47. Gattinoni L, Caironi P, Cressoni M, et al. Lung recruitment in patients with the acute respiratory distress syndrome. N Engl J Med. 2006; 354:1775–1786. [PubMed: 16641394]

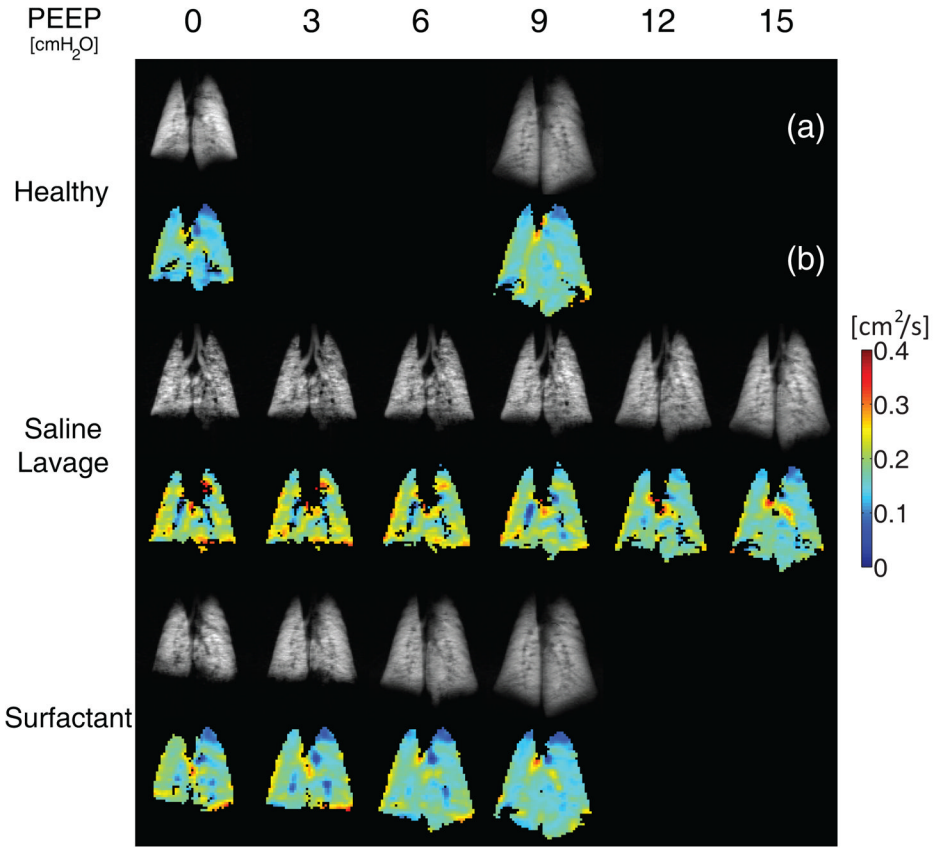

Figure 1.

Graphic outline of the experiments. After anesthesia and instrumentation, animals received baseline imaging before saline lavage (Pre-SL). Imaging was then repeated after lavage (Post-SL). Each imaging procedure was preceded by a recruitment maneuver to standardize recruitment conditions. Except for Series 1 animals, ascending levels of PEEP were applied during imaging. In Series 2 and 3, exogenous surfactant was administered and imaging was repeated for a third time. Imaging was performed using HPG-MRI in Series 1 and 2, CT was used in Series 3.

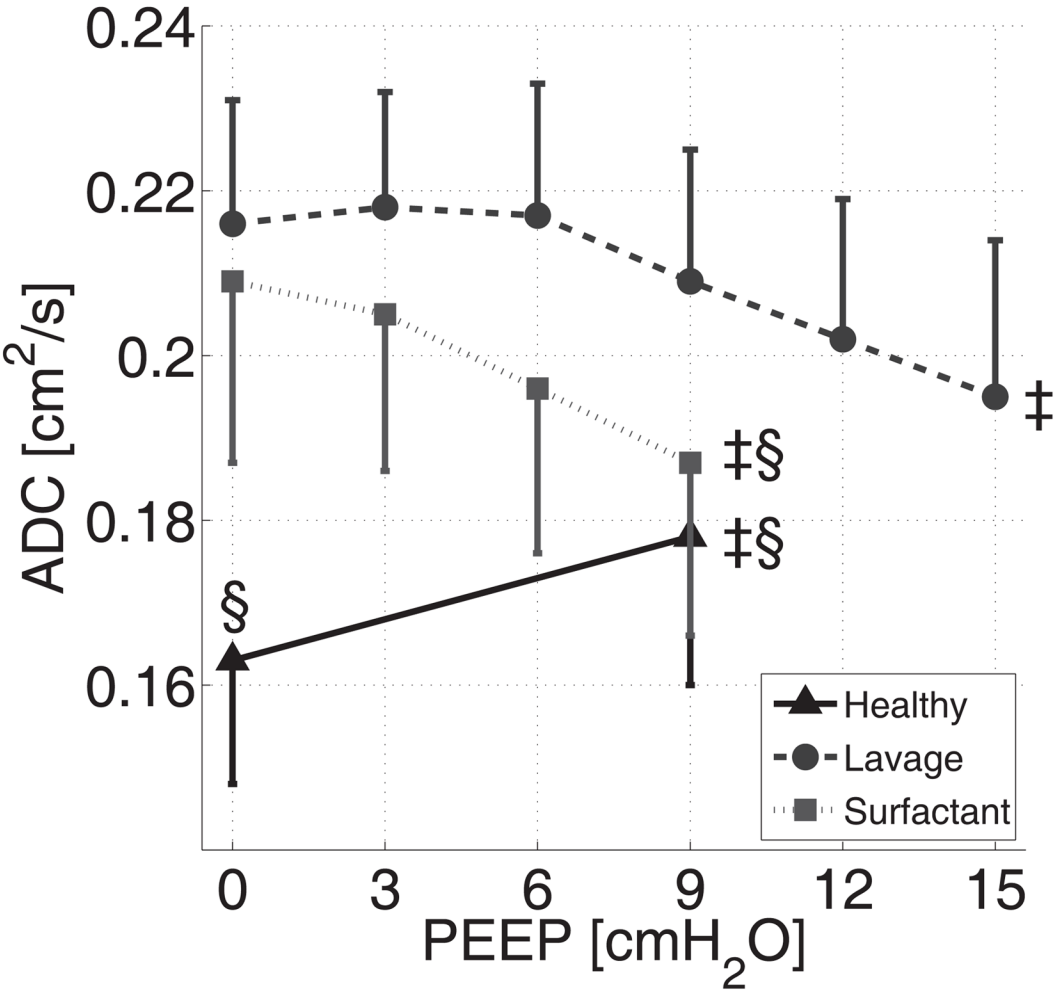

Figure 2.
^{3}He spin density maps (a), ADC (cm^2/s) maps (b), and corresponding ADC frequency distributions (c) in the mid-transverse slice obtained at baseline conditions and after saline lavage in two representative animals.

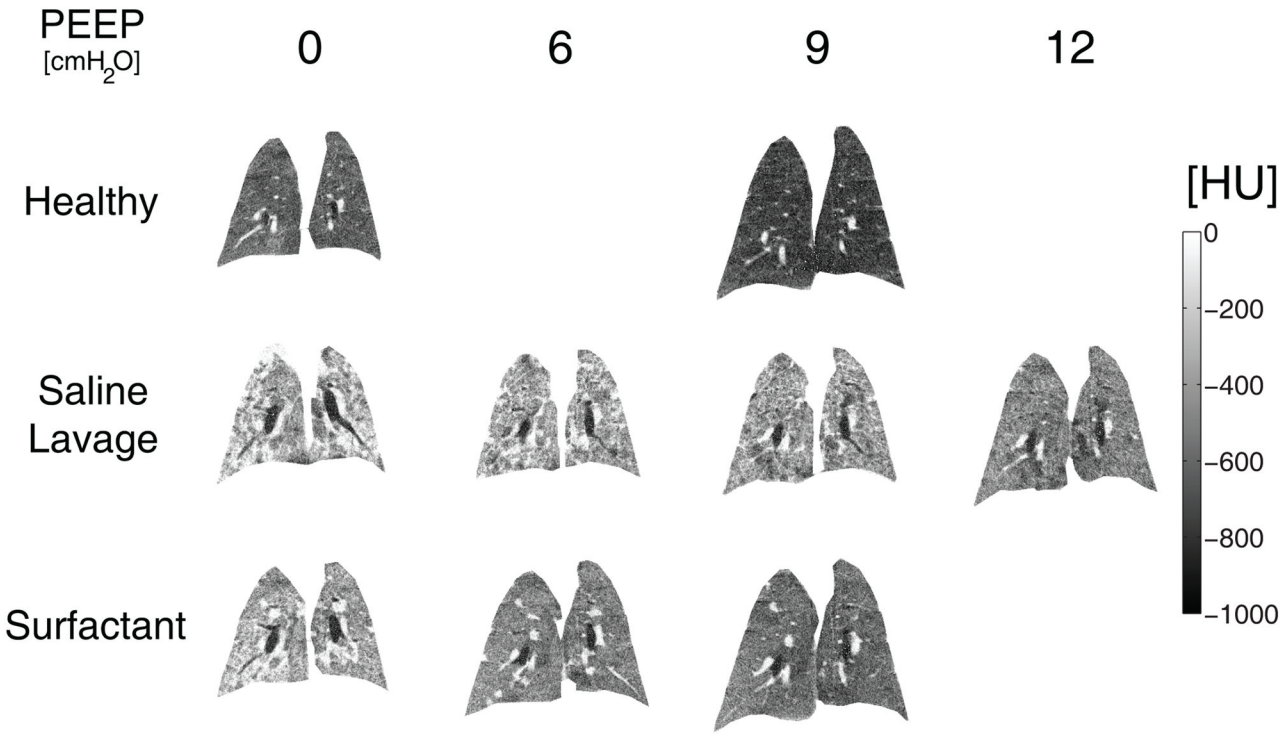

Figure 3.
High resolution ^{3}He spin density maps (a) and ADC maps (b) obtained from the posterior coronal slice in one representative animal from series 2. Images were obtained at healthy baseline, after saline lavage, and, finally after surfactant administration. Grey scale: ^{3}He density; color scale: ADC (cm^2/s).

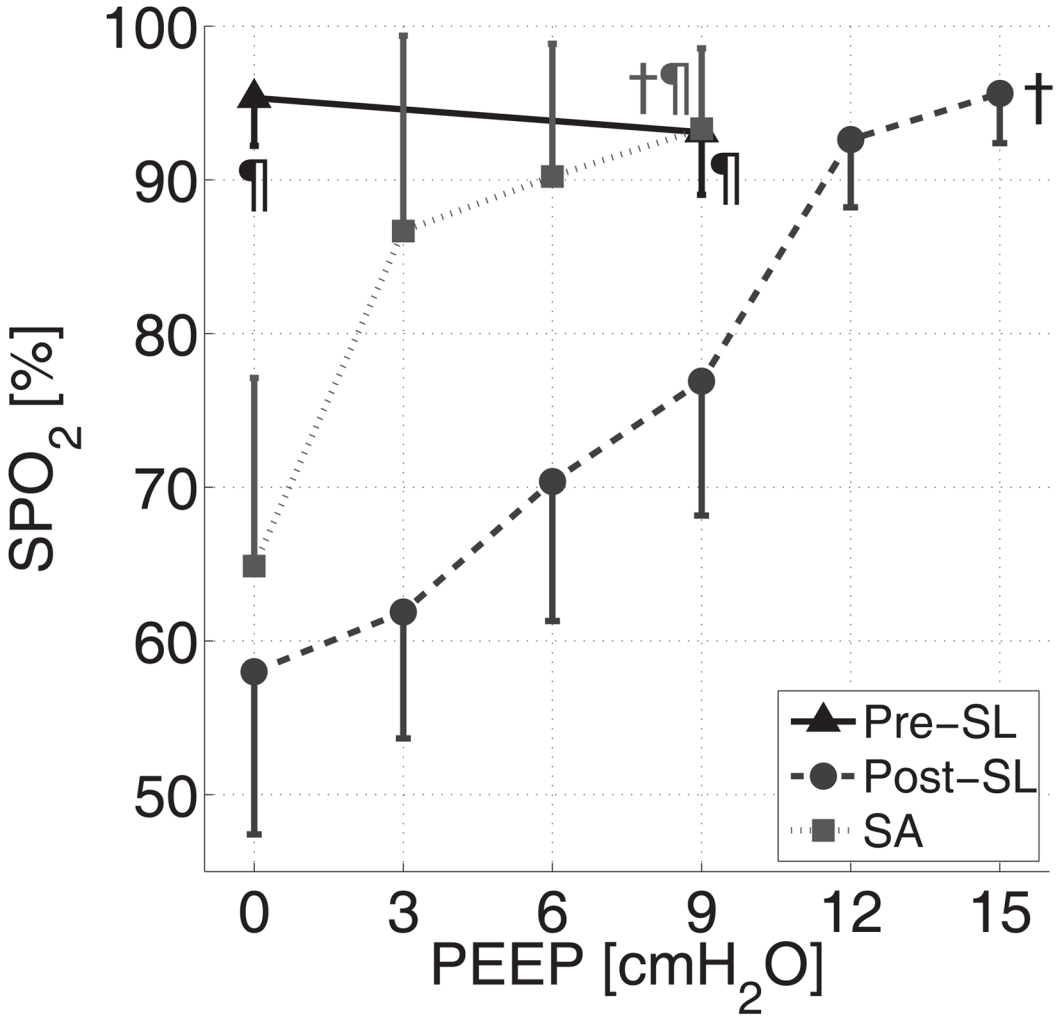

Figure 4.

Combined anterior and posterior ADC values (Mean ± SD) from series 2 rats: effects of PEEP at baseline conditions (black triangles) and after saline lavage (grey circles), followed by surfactant administration (gray squares).

‡: P<0.001 for effect of PEEP (ANOVA); §: P<0.001 vs. saline lavage at PEEP 0 or 9 cmH_2O.

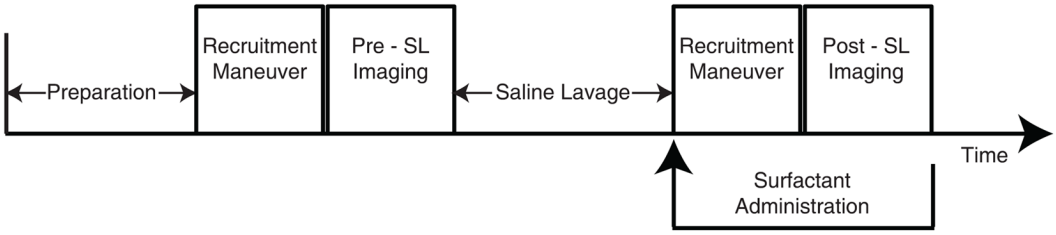

Figure 5.
Posterior coronal CT scans obtained in one animal from Series 3 at healthy baseline, after saline lavage, and after surfactant administration at different PEEP levels. HU: Hounsfield Units.

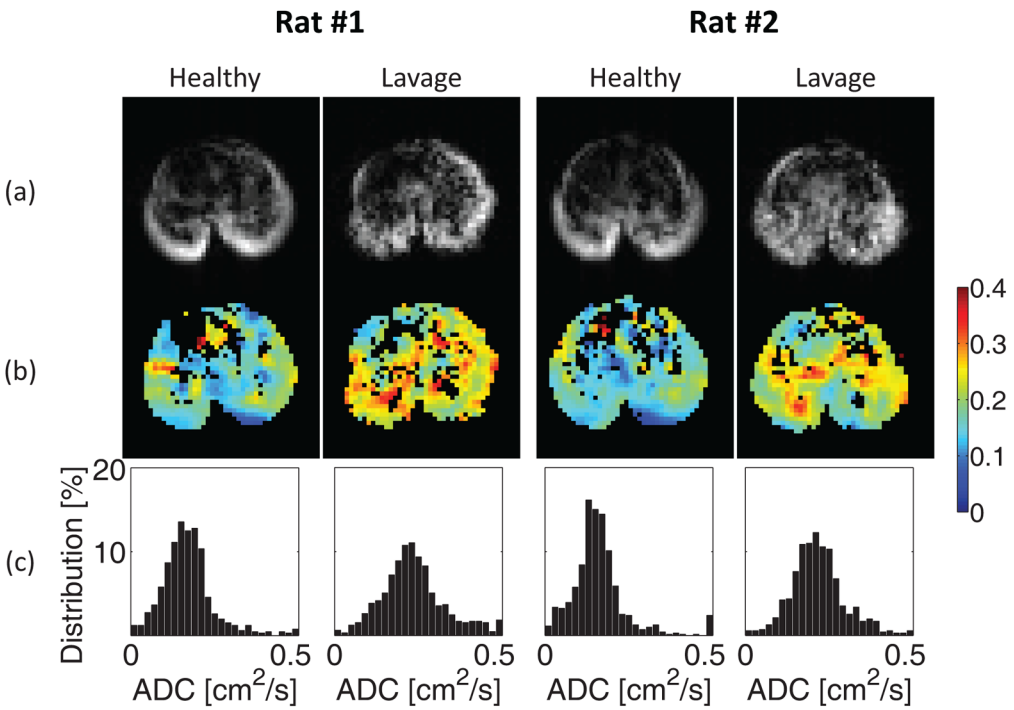

Figure 6.

Effects of PEEP at baseline conditions (black triangles), after saline lavage (grey circles), and following surfactant administration (gray squares) on the distribution of aeration density ranges (% of total slice area). Density ranges were defined as: non-aerated (≥ −100 HU), poorly aerated (−500 to −101 HU), normally aerated (−900 to −501 HU), and hyperinflated (< −900 HU). †: P<0.01 and ‡: P<0.001 for the effect of PEEP; ¶: P<0.01 and §: P<0.001 vs. saline lavage at PEEP 0 or 9 cmH_2O.

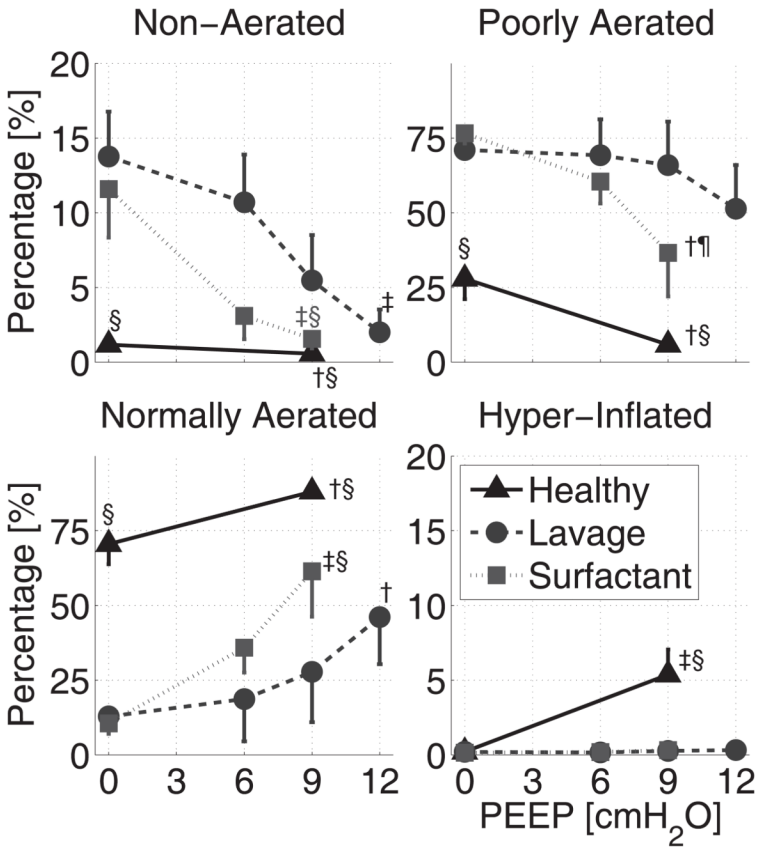

Figure 7.
Effects of saline lavage, PEEP, and surfactant administration on the peripheral oxygen saturation (SpO_2) in Series 3 animals. †: P<0.01 for effect of PEEP; ¶: P<0.01 vs post-SL.

Table 1

Group averages (± standard deviation) of variables measured in Series 1 rats.

	Baseline	Saline Lavage	P
Apparent Diffusion Coefficient, cm^2/s	0.169 ± 0.016	0.229 ± 0.012	<0.001
Peak Inspiratory Pressure, cmH_2O	8.90 ± 1.39	28.17 ± 2.79	<0.001
Dynamic compliance, mL/cmH_2O	0.464 ± 0.055	0.145 ± 0.016	<0.001
Standard Deviation[a]	0.065 ± 0.006	0.074 ± 0.005	<0.002
Skewness[a]	0.693 ± 0.249	0.156 ± 0.245	<0.001
Kurtosis[a]	4.669 ± 0.836	3.481 ± 0.356	<0.001

[a]Standard deviation, skewness, and kurtosis were obtained from the frequency distribution of apparent diffusion coefficient values within each imaged slice.